

Mechanics and rheology of basalt fiber-reinforced polycarbonate composites

Keon-Soo Jang

ICT Materials & Components Research Laboratory, Electronics and Telecommunications Research Institute (ETRI), Daejeon, 34129, South Korea



ARTICLE INFO

Article history:

Received 26 March 2018

Received in revised form

26 May 2018

Accepted 2 June 2018

Available online 4 June 2018

Keywords:

Basalt fiber

Polycarbonate (PC)

Composite

ABSTRACT

To enhance the mechanical, thermal, and electrical properties and economic profits, polycarbonates (PCs) have been blended with various inorganic additives for the past few decades. Herein, we fabricated basalt fiber (BF)-infiltrated PC composites as a promising candidate for a myriad of PC applications. Mechanical robustness and rheology were examined via the precise control of BF contents (up to 12.5 phr). The incorporation of BF gradually enhanced the mechanical properties of the composites such as moduli and strengths, as determined by flexural and tensile tests. The Izod impact strength was reduced as a function of BF concentration, representing the ductile-to-brittle transition. The heat deflection temperature of the PC/BF composites was increased from 131.2 °C to 138.9 °C, which was in good agreement with the thermomechanical results. By contrast, the glass transition temperature measured by differential scanning calorimetry remained unchanged at ca. 143 °C. The incorporation of BF in PCs enhanced the dimensional stability. The visual observation for PC/BF composites was examined via scanning electron microscopy. The rheological investigation was systematically performed by utilizing the melt flow index, and capillary and torsional rheometry with a variety of experimental conditions. These PC/BF hybrid composites with tunable mechanical and rheological properties will be employed for various applications by tailoring the PC/BF ratios.

© 2018 Published by Elsevier Ltd.

1. Introduction

Reinforcing fibers have been widely used for polymer composites, such as glass and carbon fibers [1–5]. The carbon fibers (CFs)-embedded polymer composites typically enhances the mechanical integrity, ductility, and flame retardancy and reduces the weight of polymer composites, extending to engineering applications such as space technology, aircraft industry, war industry and sports [6–9]. The major drawback of CFs is, however, their extremely high production cost, resulting in low loading capability. Instead of CFs, the most popular reinforcing fiber is glass fibers (GFs, ca. 85 wt% of reinforcing fibers), showing low coefficient of thermal expansion (CTE) and moisture resistance in the case of polymer composites [1,2]. Their overall mechanical properties are somewhat lower than that of the carbon fiber [2]. However, GFs are much more inexpensive than CFs.

Recently, basalt fibers (BFs) have been examined due to similar mechanical properties and lower production cost, compared with

glass fibers [10,11]. The BFs are extruded from igneous basalt-based volcanic rock, which is energy efficient and simpler than any other fiber without using an additive. Unlike GFs, BFs contain more components such as SiO₂, Al₂O₃, CaO, MgO, Fe₂O₃, FeO, TiO₂, K₂O, and Na₂O than GFs [10]. These various components provide large, complex crosslinked architecture, resulting in excellent chemical resistance under corrosive environments. They are also thermally stable, non-toxic, natural, and eco-friendly [10]. BFs have been employed in several thermoplastic polymers such as polypropylene (PP), polylactide (PLA) and poly(butylene succinate) (PBS) [12–14]. The mechanical properties of BF-embedded PP, PLA and PBS were primarily investigated. The incorporation of BFs into these three polymers enhanced their tensile strengths and moduli; however, it reduced the Izod impact strength. These researches have narrowly dealt with rheological properties [12–14].

Polycarbonates (PCs) have gained a myriad of applications, ranging from home appliances to the aerospace industry due to the excellent balance of optical transparency, mechanical robustness, heat resistance, impact strength, and electrical properties [15–17]. For high-performance PC applications such as the aviation industry, high-performance additives are embedded. Meanwhile, for general

E-mail addresses: ksjang4444@etri.re.kr, ksjang4444@gmail.com.

applications, low-cost mineral fillers are widely utilized to reduce the cost of the final product. Furthermore, PCs with low CTE are highly required for most electronic devices where thermal gradient and temperature fluctuations during the operation lead to substantial dimensional change, thereby causing distortion. The incorporation of inorganic mineral fillers can substantially reduce the CTE of the polymeric composites [18–20]. In particular, inorganic fibrous materials in a polymeric matrix are preferentially aligned along the flow direction, leading to significant reduction in the CTE along the flow direction [18,19]. The inorganic fibers also enhance the mechanical properties of PCs although toughness or strength impact is typically sacrificed as the ductile behavior of the moderate molecular weight PCs lies in the unique ductile-to-brittle transition region [21–23]. Several research groups have reported GF-reinforced PC composites [24–26]. However, BF-embedded PC (PC/BF) composites have not been reported to date. In this research, the rheological and mechanical properties of PC/BF composites were explored.

2. Experimental

2.1. Materials

Two different PC grades, SC-1080P (pellet, MFI = 8 g/10 min at 300 °C/1.2 kg) and SC-1190G (granule, MFI = 19 g/10 min at 300 °C/1.2 kg) were obtained from Samsung SDI Co. Some additives such as internal and external lubricants (long-chain ester of pentaerythritol and high density polyethylene wax), a thermal stabilizer/primary antioxidant (stearate-based hindered phenol), and a secondary antioxidant (phenyl-functionalized phosphite) were utilized to facilitate extrusion and injection processing. It should be noted that sulfonate salt-, phosphate-, bromine- and silicone-based flame retardants are typically used with thermally shrinkable anti-dripping additives such as polytetrafluoroethylene (PTFE) for PCs and mineral filler/PC composites [15]. However, herein, these flame retardants were excluded to concentrate on the inherent effect of BFs. BFs (Kamenny Vek Co. Russia) with a diameter of 20 μm and length of 5 mm were used as received. Chloroform (CHCl₃, 99%) was purchased from Sigma-Aldrich.

2.2. Composite fabrication

For twin screw extruders, pellet and granule types are commonly used together to avoid layer separation during hopper feeding since most additives such as antioxidants, light stabilizers, internal lubricants, external lubricants, impact reducers, and flame retardants are fine powders [15]. Thus, the pellet (5.0 kg) and granule (5.0 kg) PC resins, the internal (0.2 phr) and external (0.2 phr) lubricants, the thermal stabilizer (0.3 phr), and the secondary antioxidant (0.2 phr) were mixed together with a tumbler mixer at 20 rpm for 10 min. Subsequently, the mixture was fed into a main hopper of an intermeshing corotating twinscrew extruder at the hopper temperature of 100 °C at a rate of 40 kg/h. Meanwhile, the BFs were fed through a side feeder at an associating feeding rate (2.5–12.5 phr) to minimize fiber breakage. The PC/BF composites composed of 2.5 phr BF via a side feeding zone (SFZ) are referred as PC/BF2.5-SFZ (or PC/BF2.5) hereafter. For comparison, all materials including BFs and PCs were also fed together via a main feeding zone (MFZ) as shown in Scheme 1. PC/BF2.5-MFZ denotes the composite containing PC with 2.5 phr BF extruded via main feeding zone (MFZ). The extruder barrel temperatures from the feed zone to the die were maintained at 260 °C. The rotational speed of the extruder screw was 200 rpm. The screw diameter and the length-to-diameter ratio were 45 mm and 36, respectively. The polymer melt extrudates from the die were cooled down by using a room-

temperature water bath, and pelletized at the end. The pelletized composites were dried at 80 °C for 4 h prior to the injection molding. Measurement specimens for tensile, flexural, notched Izod impact strength, and heat deflection temperature (HDT) tests were fabricated by injection molding at a barrel temperature range of 220–260 °C and a mold temperature of 60 °C.

2.3. Characterization techniques

Tensile tests were carried out using an Instron mechanical tester (Model 5580), in accordance with ASTM D638. A crosshead rate of 5 mm/min was selected due to the infiltrated BFs. The flexural strength and modulus were obtained using a three-point flexural test at a crosshead rate of 2.8 mm/min, according to ASTM D790. The tensile and flexural tests were performed at room temperature. The mean values of tensile and flexural results were determined from five specimens for each composite with different BF contents.

Notched Izod impact strength was obtained according to ASTM D256 at a thickness of 3.2 mm at room temperature. The mean value was determined among 10 specimens for each composite.

0.5 g of the PC/BF12.5 composite was dissolved in 40 mL of chloroform. Subsequently, the fibrous precipitate was filtered and carefully washed with 40 mL of chloroform five times. The mean fiber length and the length distribution were measured on the basis of OM images using Image J software.

Optical microscopy (OM, Microphot-FXA, Nikon) equipped with a digital camera was employed to measure the fiber length and its distribution after the compounding process. The light source was 12 V–100 W halogen lamp (Philips 7724) controlled by the BioRad MRC-600 computer software program, COMOS[®] (BIO-RAD Lab.).

The morphology of the reinforced composites was investigated via scanning electron microscopy (SEM, Model S-4800, Hitachi) at an electron beam voltage of 10.0 kV. The fractured composite samples for SEM were prepared from the Izod impact strength tests. The PC/BF12.5 composite surface parallel to the machine direction was obtained by fracturing a tensile specimen in liquid nitrogen. The fracture surface was coated with a 5 nm thick gold layer using a sputter coater for elevated conductivity prior to SEM observation.

The PC/BF ratio was monitored by using a polymer burn-off test (also referred to as ashing) at 750 °C for an hour. The weight of residue after ashing was converted into the weight fraction.

To verify the ratio, the specific gravity was also measured according to ASTM 792 (water displacement method).

HDT was measured with a Toyoseiki 6A-2, based on ASTM D648 at a heating rate of 2 °C/min and with a load of 1.82 MPa. The specimen was immersed under load in a heat transfer medium. The temperature of the medium was determined to be HDT when the test bar has a deflection of 0.254 mm (0.1 in).

Differential scanning calorimetry (DSC, TA Ins. Model Q20) was conducted to identify the glass transition temperatures of the composites at a scanning rate of 10 °C/min under nitrogen purging (50 mL/min). The samples were pre-heated at 250 °C for 5 min to minimize the thermal history and then cooled down to room temperature at 10 °C/min. Approximately 5.0 mg of reinforced composites in a hermetic aluminum pan was used.

The CTE was measured by thermomechanical analysis (TMA) with 0.02 μm and 9.8 μN load displacement resolution (TMA6100, Seiko Exstar 6000). The thickness of all specimens and the heating rate for the TMA tests were approximately 3.2 mm and 10 °C/min, respectively.

Melt flow index (MFI), also referred as MI was measured at 250 °C with a load of 10 kg, based on the standard test method, ASTM D1238. The piston diameter, nozzle (orifice) diameter, and nozzle length were 9.5, 2.1, and 8.0 mm, respectively.



Scheme 1. Screw configuration by assembling diverse screw elements (conveying, kneading, mixing and sealing) on screw shafts in a modular design. MFZ: main feeding zone. SFZ: side feeding zone.

Chemorheological behavior was investigated by a torsional parallel plate rheometer (HAAKE MARS III, Thermo Scientific Inc.), using 20 mm disk geometry and 1.0 mm sample gap. The dynamic viscoelastic properties of the reinforced composite melts were monitored at $\tau = 1$ Pa in the frequency ranging from 0.01 Hz to 100 Hz at three different temperatures (250, 260 and 270 °C).

The shear viscosity of the reinforced composites for the high shear rate (50 to 10^4 s^{-1}) was evaluated via capillary rheometry at 270 °C. The pellet specimens were loaded and maintained at 270 °C for 10 min to induce thermal equilibrium. The barrel was equipped with three heating elements, controlling the accurate temperature of the barrel. The temperature deviation was ± 0.3 °C during measurement. However, it should be noted that for polymer melts at high processing rates, the Nahme-Griffith number (Na , the ratio for the rate of heat generation by frictional dissipation relative to that of heat loss via conduction) is not negligible due to the elevated viscosity and low thermal conductivity of polymers [27,28]. The Na of PC is usually >1 at higher shear rates (>400 s^{-1}) and thus the viscous heating effect is not negligible [27,29]. In addition, at a length to radius (L/R) of capillary tube <200 , entrance pressure drop may influence the measurement accuracy and the measured viscosity via capillary rheometry is the apparent viscosity. Therefore, Bagley correction was used, by plotting the pressure drop vs. L/R ratio.

3. Results and discussion

Due to the limited capability of the side feeder during extrusion and nature of the BF, a BF concentration higher than 15 phr was hardly side-fed, thereby showing unexpected PC/BF ratios. Thus, to investigate the maximal effective concentration of BF on mechanics, the BF was also fed with PCs together via the MFZ.

Tensile and flexural properties such as strength and modulus are routinely considered to represent the mechanical robustness of polymeric composites. The tensile and flexural moduli of PC/BF composites at various ratios are shown in Fig. 1a. The composites were extruded with BFs fed via the MFZ and SFZ. For PC/BF-SFZ, the tensile and flexural moduli were gradually increased from 2.3 to 2.2 GPa to 3.9 and 3.8 GPa, respectively, as a function of BF content ranging from 0 phr to 12.5 phr. On the other hand, the tensile and flexural moduli of PC/BF-MFZ were slightly increased from 2.3 to 2.2 GPa to 2.8 and 2.9 GPa, respectively with increasing BF concentration from 0 to 12.5 phr. Further incorporation of BF slightly enhanced the tensile and flexural moduli up to 3.7 GPa and 3.8 GPa, respectively. Above 40 phr, an insignificant difference in both moduli was observed. The moduli of PC/BF12.5-SFZ were higher than those of PC/BF12.5-MFZ due to smashed BF during extrusion (Figure S1). The fiber length for PC/BF12.5-SFZ and PC/BF12.5-MFZ, and its distribution after the compounding process were measured on the basis of OM images (Figure S1) since they influence the mechanical and the rheological properties of the composites [32]. The mean fiber length of PC/BF12.5-SFZ and PC/BF12.5-MFZ was determined to be 680 ± 180 μm and 165 ± 104 μm , respectively (Figure S2). These results are in good agreement with the Einstein-Guth-Gold equation [30,31].

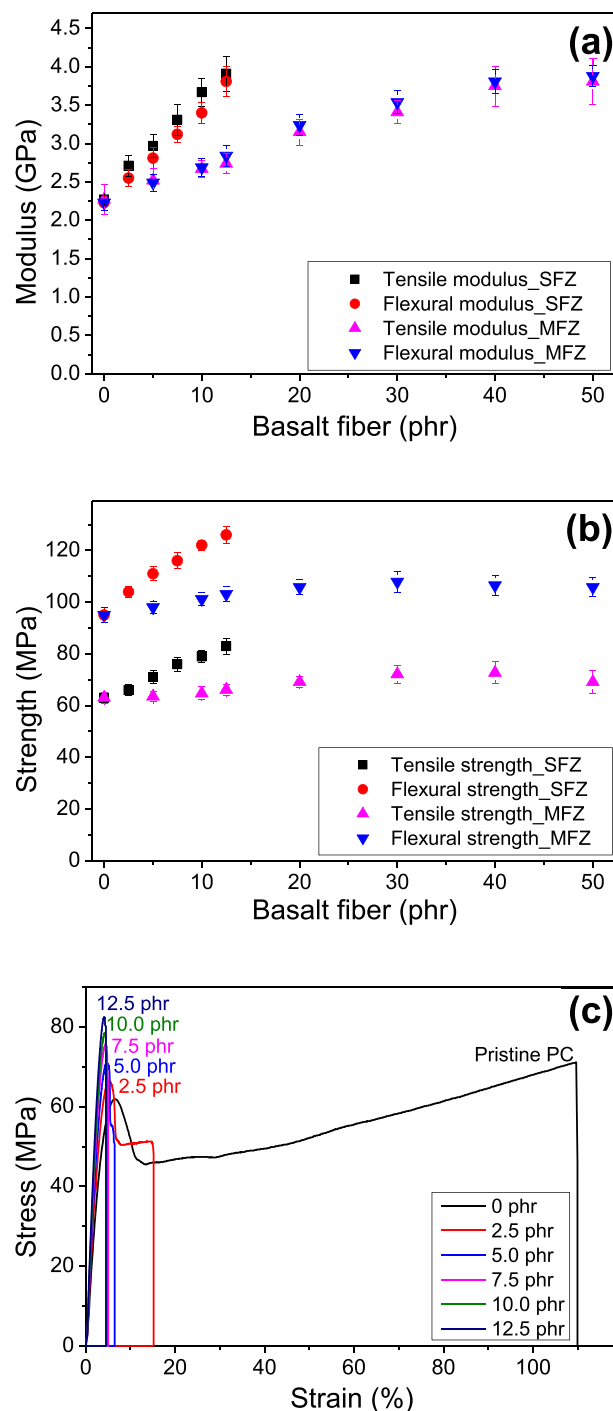


Fig. 1. Tensile and flexural moduli (a), tensile and flexural strength (b) of PC/BF composites, and tensile stress-strain curve (c) of PC/BF-SFZ composites.

$$E = E_0 (1 + 0.67f\Phi + 1.62f^2\Phi^2) \quad (1)$$

where E and E_0 are the tensile moduli of the fibrous composites and pure polymeric matrix, respectively; f is the ratio of length to diameter of the inorganic fibrous material; and Φ is the fiber volume fraction.

Similar to the moduli results, the tensile and the flexural strengths of PC/BF-MFZ were only slightly increased from 63 to 95 MPa to 66 and 103 MPa, respectively with a fiber content range of 0–12.5 phr. Subsequently, the strengths were somewhat enhanced to 73 and 107 MPa, respectively by further incorporation of BFs up to 30 phr. Beyond 30 phr, those were maintained. By contrast, the strengths of PC/BF-SFZ composites were steadily increased from 63 to 95 MPa to 83 and 126 MPa, respectively, with the same fiber concentration range of 0–12.5 phr, as shown in Fig. 1b. Based on the mechanical tests performed above, the PC/BF-SFZ composites with BFs side-fed during extrusion were preferable to the PC/BF-MFZ composites and thus the PC/BF-SFZ composites are explored hereafter (PC/BF denotes PC/BF-SFZ from here on). It is also assumed that the BF carries the load, and stress is transferred from the polymer matrix along the fibrous inorganic filler, bringing about good stress distribution and enhancing mechanical robustness. The large difference between the tensile and flexural strengths may result from the rectangular shape of tensile samples. In the case of a circular or square sample shape, the ideal ratio between the tensile and flexural strengths is 1.0. Fig. 1c shows the stress-strain tensile curve for each sample. The incorporation of even 2.5 phr BF into the PC induced the ductile-to-brittle transition, which is confirmed by the study of Izod impact strength hereafter.

Either HDT or Vicat softening temperature (VST) exhibits crucial thermal information, which usually determines the injection or the compression molding conditions such as the mold temperature and pressure that determine the quality of the product surface. The VST is routinely employed for unfilled polymeric materials, whereas the HDT is suitable for inorganic filler-embedded polymeric composites due to the measurement mechanism. The HDT of BF-infiltrated composites was gradually increased from 131.2 °C to 138.9 °C with increasing BF contents from 0 phr to 12.5 phr. This increment is probably caused by mechanical robustness of the inherent BF, the anisotropic orientation of BF perpendicular to the stress direction, and interfacial bonding adhesion (non-covalent interactions, further enhanced by similarity: partially hydrophilic nature of PC and BF) between the fibrous inorganic filler and the polymeric matrix. Meanwhile, the glass transition temperatures (T_g s) measured by DSC were maintained at ca. 143 °C regardless of the BF concentration because the HDT is dependent on the mechanical response while T_g by DSC is based on calorimetry. It is well-known that the infiltration of even low filler concentration (<5 phr) into PCs leads to the ductile-to-brittle transition because high-modulus inorganic fillers act as stress concentration, thereby reducing ductility [33,34]. Furthermore, the small loading of embedded filler hinders the in-chain rotation and bending of the flexible carbonate group, and decreases interactions between backbones of PCs, thereby obstructing microfilament formation, which is contributable to the yielding mechanism. Despite these, high filler loading commonly takes place in various applications due to other mechanical and chemical stabilities, and economical aspect. As shown in Fig. 2, the Izod impact strength was dramatically reduced even at 2.5 phr of BF loading, suggesting the ductile-to-brittle transition. Above 7.5 phr loading, the Izod impact strength was slightly increased as a function of BF content. The impact strength usually tends to increase in the brittle region of PC matrix due to the different mechanism to dissipate the impact energy and fiber-

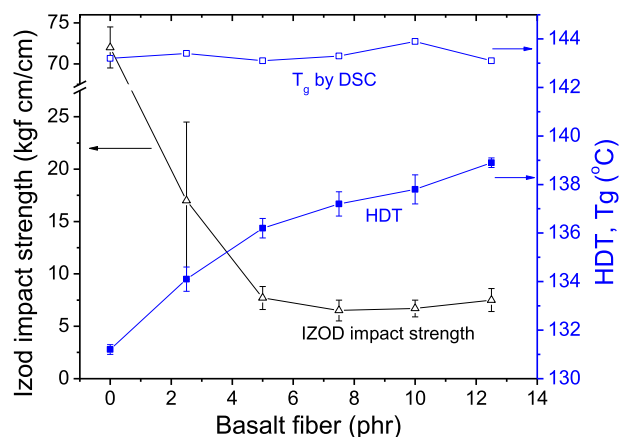


Fig. 2. HDT, T_g measured by DSC, and Izod impact strength of PC/BF-SFZ composites at various ratios.

matrix interactions such as debonding, sliding, and fiber pullout [13].

The dimensional stability of polymeric composites has been regarded as one of the most important factors especially for injection molding. The dimensional change can be determined by the CTE of materials [35,36]. Various methods, such as TMA, strain gages and differential dilatometer, have been utilized to measure

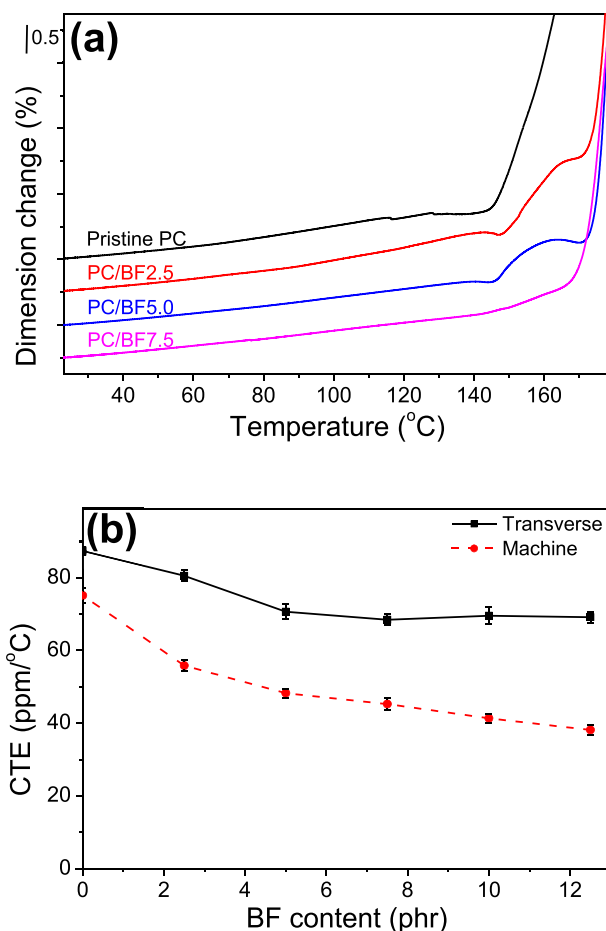


Fig. 3. Dimensional change with increasing temperature (a) and CTE of PC/BF composites for machine and transverse directions with different BF contents (b).

the CTE. The TMA is facile, fast, and suitable for small-sized specimens despite its incapability to measure CTEs in volume. As shown in Fig. 3, two different methods, namely the machine (flow direction) and transverse directions (perpendicular to flow direction) were adopted depending on the flow direction during injection molding process. The drastic slope change in the curve of dimensional change vs. temperature indicates a thermomechanical transition temperature of materials. The transition temperature shifted toward higher temperatures as a function of BF content (Fig. 3a), which is in good agreement with the HDT results although the T_g showed no change as discussed above (Fig. 2). The CTEs of PC/BF composites for the transverse and machine directions were reduced from 75.0 to 87.3 ppm/°C to 44.0 and 69.1 ppm/°C with increasing BF concentration, respectively (Fig. 3b). A larger reduction in the CTE was observed for the composites in the machine direction, compared to that in the transverse direction. The difference in CTEs is caused by the fiber orientation. The fibrous materials are typically aligned along with the flow direction. Thus, the fiber/polymer composites in the machine direction showed lower CTEs while those in the transverse direction rarely enhanced the dimensional stability, compared to the pristine polymer.

Visual observation of the fractured surface for fiber-reinforced polymer composites has been routinely observed by SEM [13,14]. Fig. 4 shows the SEM micrographs of the fractured PC/BF composites with fiber contents of 5 (Fig. 4a, c) and 10 phr (Fig. 4b, d). The uneven surface morphology may result from interfacial bonds between the fibers and the matrix, suggesting the gradually increased HDT of the composites with increasing fiber loading. The surface morphology rarely varied significantly between 5 and 10 phr of BF loading. The fibers are well dispersed through the polymeric matrix without aggregation.

For polymer processing such as extrusion and injection molding, rheological understanding is necessary to facilitate the processing and to manufacture a final product with high quality. The MFI is a facile measurement method that typically provides rheological information such as viscosity in the medium shear rate region at the shear stress-shear rate curve for most polymers. As shown in Fig. 5, the MFI was initially increased with 2.5 phr BF, suggesting a decrease in viscosity. The MFI results were inconsistent above 2.5 phr. The fibrous shape usually impedes the melt flow, thereby increasing viscosity [37]. The increment rate is dependent on the

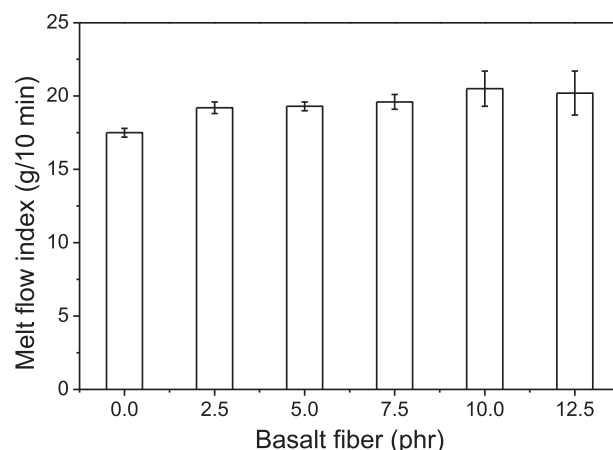


Fig. 5. MFI of PC/BF composites at various ratios.

fiber type, length, orientation and aspect ratio. The shear stress and rate applied to the polymer composites during the MFI measurement can be calculated from Equations (2) and (3).

$$\tau = \frac{R_N F}{2\pi R_p^2 l_N} \quad (2)$$

$$\dot{\gamma} = \frac{4Q}{\pi R_N^3} \quad (3)$$

where R_p , R_N , l_N , F , and Q represent piston radius, nozzle radius, nozzle length, force (test load, $\text{kg} \times 9.8 \times 10^5 \text{ dyn}$), and volume rate through the nozzle ($\text{MFI}/600\rho$, cc/s), respectively. In the case of ASTM D1238, R_p , R_N and l_N are 0.47, 0.1 and 0.8 cm, respectively. Thus, the shear stress and strain become simplified as shown in Equations (4) and (5). Merging these equations, the final equation (Eq. (6)) regarding viscosity vs. MFI can be obtained.

$$\tau = 9.13 \times 10^4 L \quad (4)$$

$$\dot{\gamma} = 1.83 \times \text{MFI}/\rho \quad (5)$$

$$\eta \times \text{MFI} = 4.98 \times 10^4 \rho L \quad (6)$$

The measured MFI at a certain force (test load) can be converted to either the shear rate or the viscosity, according to Equations (5) and (6).

Due to the unique rheological properties of polymers and their composites such as shear thinning behavior, it is of great importance to investigate viscosities with a wide range of shear rates for associating processing methods. The shear viscosity at high shear rate (10^3 to 10^6 s^{-1}), involved with roll coating, spraying, extrusion, and injection molding (in particular, small gates and runners) is routinely measured by capillary rheometry, which is one of the most commonly used rheological measurements [38]. The fundamental theory of the capillary rheometer is similar to that of the MFI measurement. For inorganic filler-embedded polymeric composites, the architecture, dimension, orientation, and concentration of inorganic fillers affect the rheology of the polymeric composite melt. The incorporation of inorganic fillers into polymer matrices induces shear thinning behavior at high shear rates, which are ascribed to the processing conditions for injection molding, roll casting and spraying [38]. The magnitude of shear thinning determines the process windows. At a relatively low shear rate region, the viscosity of the composites, however, commonly increases as a

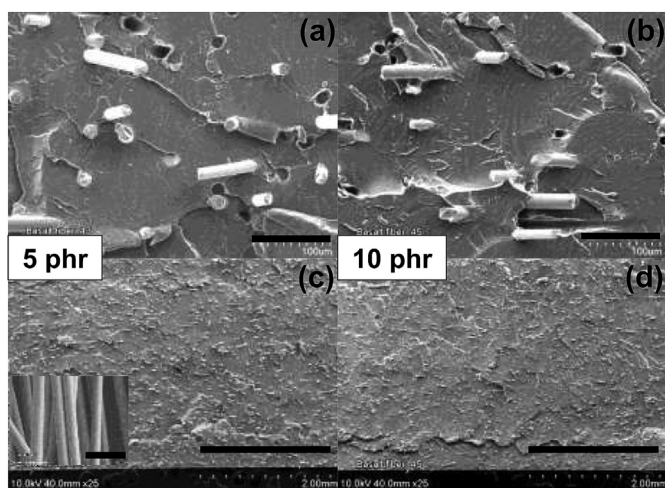


Fig. 4. Fracture morphology of PC/BF composites via SEM: 5 phr (a, c), 10 phr (b, d). The inset indicates pure fibers before being embedded into the PC matrix. Scale bars for a, b, and c, d are 100 μm and 2.0 mm, respectively. The scale bar in the inset represents 50 μm .

function of filler content [37]. Fig. 6 also shows the shear thinning phenomenon for all composites at the whole frequency ranges and rare gap in viscosity between the neat polymer matrix and the BF-infiltrated polymeric composites at high shear rates. The analogous viscosity at high shear rates was caused by the alignment of the fibrous shape along the flow direction (Figure S3) and slip between the fibers and the polymeric matrix. Thus, the rheological hindrance becomes minimized. It should be noted that the chain scissor caused by the incorporation of inorganic fibrous filler may occur at a high temperature at a high shear rate, thereby reducing the viscosity. The chain scissor is also involved in Fries rearrangement and Kolbe-Schmitt rearrangement at high temperatures [39].

The shear viscosity for mixing, blade coating, compression molding, extrusion blow molding, and brushing is involved with the shear rate ranging from 100 to 10^2 s^{-1} while the shear viscosity for sagging and leveling is related to the range from 10^{-3} to 10^{-1} s^{-1} . This wide range at low shear rate region can be measured by torsional rheometry equipped with parallel circular plates mounted between an actuator (transducer) and a fixture, to characterize the rheology of fiber suspensions at low shear rates. The rheological behaviors of fiber-reinforced composites are often dependent on the measurement temperature. The viscosity, and the storage (G') and loss (G'') moduli tend to decrease as a function of temperature. The complex viscosity, G' and G'' decreased with increasing temperature at frequencies ranging from 0.01 s^{-1} to 10^2 s^{-1} , exhibiting similar rheological curves, as shown in Fig. 7a–c, respectively. The complex viscosity was decreased at low shear rates and increased at high shear rates above 30 s^{-1} , indicative of shear thickening behaviors owing to the elevated slope of G' vs. the shear rate beyond ca. 0.7 s^{-1} , and drastic reduction in G'' at high shear rates as shown in Fig. 7b and c, respectively. Moreover, considering that the rate of fiber rotation is involved with the shear rate, inhomogeneity along shear fields may elevate the fiber-fiber interaction during transient changes in the fiber microstructure.

The incorporation of inorganic fillers into a polymeric matrix influences the rheological properties, depending on the sizes, shapes, concentrations and chemical structures of the inorganic fillers, and shear rates. For instance, the viscosity of spheric fillers-embedded composites decreases with increasing filler content whereas that of fibrous fillers in polymers increases [27]. The infiltration of CaCO_3 into polymeric matrices such as polypropylenes and PCs commonly induces chain scission at high temperature ($>250 \text{ }^\circ\text{C}$), thereby reducing viscosity [40]. Fig. 8a–d shows the rheology of neat PC matrix and BF-reinforced PC composites. Fibrous architecture generally hinders the melt flow especially at

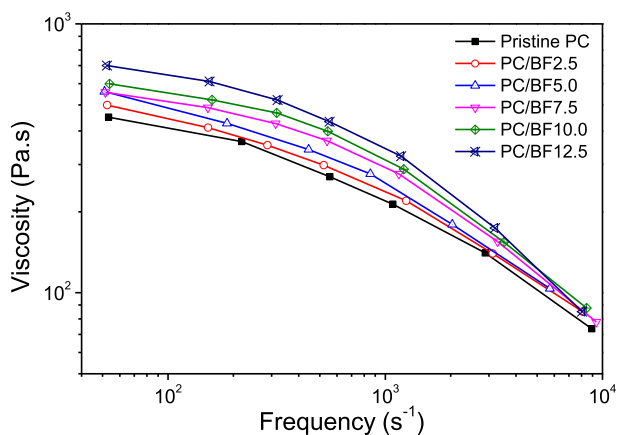


Fig. 6. Apparent viscosity vs. shear rate for PC/BF composites at $270 \text{ }^\circ\text{C}$ measured by capillary rheometry.

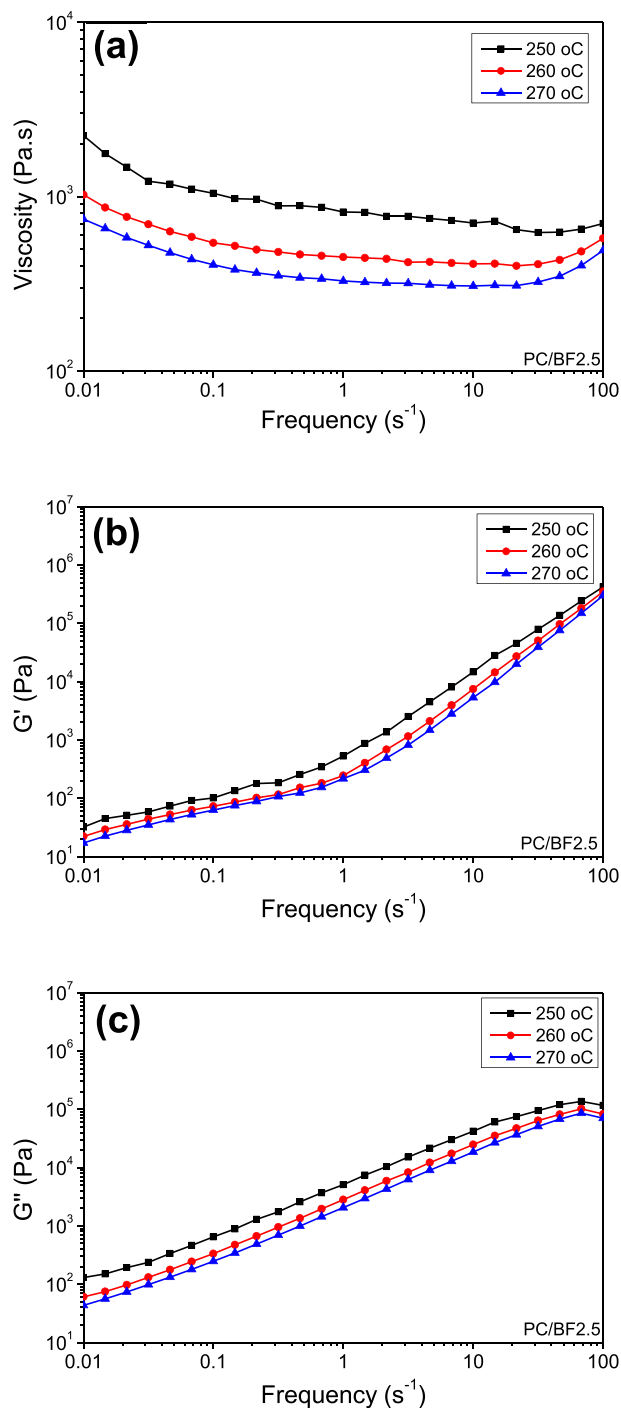
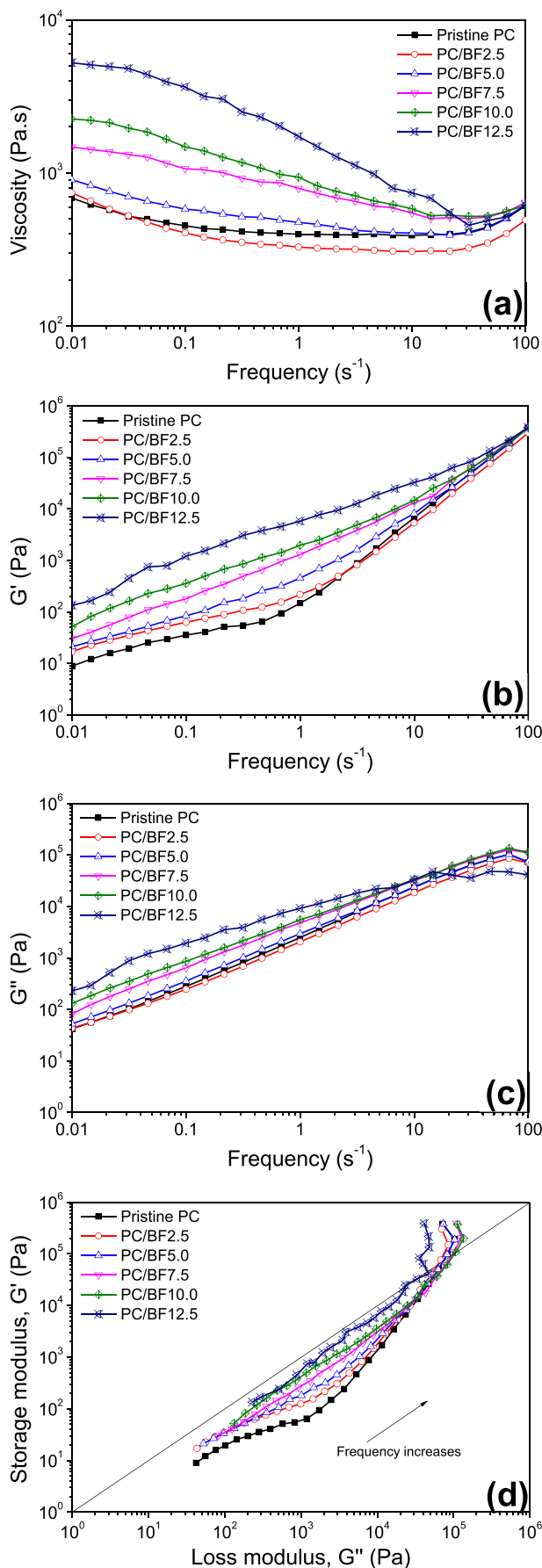


Fig. 7. Complex viscosity (a), shear storage modulus (b), and shear loss modulus (c) of reinforced composites embedded with 2.5 phr of BF in frequency ranging from 10^{-2} to 10^2 s^{-1} with different temperatures.

low shear rates. The complex viscosity of the reinforced composites tends to significantly increase as a function of BF concentration at low shear rates primarily due to the elevated G' in Fig. 8a and b. The corresponding increment in G'' is lower compared to G' as shown in Fig. 8c. Meanwhile, the analogous viscosity for all composites was measured at high shear rates. Shear thinning behaviors for all samples were observed from 10^{-2} to 30 s^{-1} . Above these values, all samples showed shear thickening behaviors, which may be caused by the phase separation of the added lubricants due to the torsional



vibration at high shear rate. It should be noted for experimental consideration that various conditions including the controllable stress mode and displacement mode with a myriad of values ($\tau = 0.01\text{--}50$ Pa and $\gamma = 0.01\text{--}20$) were performed from 1 to 100 s^{-1} to ensure the unexpected shear thickening behavior of all the composites. The magnitude of shear thinning effect for the highest concentration (12.5 phr) of PC/BF composites was larger than any other samples due to the possibility that more fibers for the PC/BF12.5 composite are aligned along the melt flow direction (Figure S3), bringing about a larger gap in viscosity, relative to the case of low BF loading. Interestingly, the slope of shear storage modulus vs. frequency slightly changed around 0.7 s^{-1} from the pristine PC up to the PC/BF5.0 composite. Beyond this point, the slope remains unchanged, suggesting that the elasticity of the composites composed of high BF concentrations was more stabilized along the whole frequency.

Fig. 8d shows a plot of G' vs. G'' with a frequency parameter, which is ascribed to the Cole-Cole plots employed for dielectric spectroscopy [41]. Such plots can be utilized to examine the microstructure of polymers including copolymers and blends with different temperatures [42,43]. The curves of G' vs. G'' at different temperatures coincide in the case of stationary microstructure of the single phase melt. On the other hand, the curves transition parallel in the event of tunable microstructure. In addition to the case involving tunable temperature conditions, such plots can be harnessed to probe the structural alterations at a fixed temperature. For instance, modified Cole-Cole plots were employed to investigate the branching and the molecular weight distribution of polyethylene on the microstructure [44]. The G' was more enhanced compared to G'' with increasing long chain branching. This analytic investigation can be also conducted for composites such as rubber-embedded acrylonitrile-butadiene-styrene (ABS) composites, representing the enhanced elasticity of the matrix with increasing rubber contents [45]. As shown in Fig. 8d, the shear storage modulus at a certain shear loss modulus increased as a function of BF. G' was lower than G'' for all the samples at a wide range of frequencies. Finally, G' transitions dominant over G'' at high shear rates, leading to higher viscosities and thus shear thickening behaviors (Fig. 8a).

To facilitate the quantification of the fibrous effect on rheology, Fig. 8a–c were converted to Fig. 9a–c where the complex viscosity, G' and G'' for each frequency from 0.01 s^{-1} to 100 s^{-1} are plotted as a function of BF content. The complex viscosity of PC/BF composites increased with increasing BF contents from 0.01 s^{-1} to 10 s^{-1} (Fig. 9a). At lower shear rates, the slope (ratio of viscosity to BF content) was more precipitous. At 100 s^{-1} , the viscosity was insignificantly changed, suggesting that the BF effect becomes minimized at high shear rates. G' and G'' indicate similar behavior in terms of the slope to the complex viscosity at 100 s^{-1} . G' and G'' for all composites were enhanced as a function of shear rate while the complex viscosity showed different behaviors at 100 s^{-1} .

4. Conclusion

By incorporating BFs into a PC matrix, the mechanics was significantly enhanced except for the impact strength. The rheological properties were explored by MFI, and capillary and torsional rheometry with various temperatures and a wide range of frequencies. The tensile and the flexural modulus were gradually enhanced from 2.3 to 2.2 GPa to 3.9 and 3.8 GPa, respectively, up to

Fig. 8. Complex viscosity (a), shear storage modulus (b) and shear loss modulus (c) vs. shear rates ranging from 10^{-2} to 10^2 s^{-1} , and G' vs. G'' (d) at 270 $^{\circ}\text{C}$ for neat PC matrix and PC/BF composites.

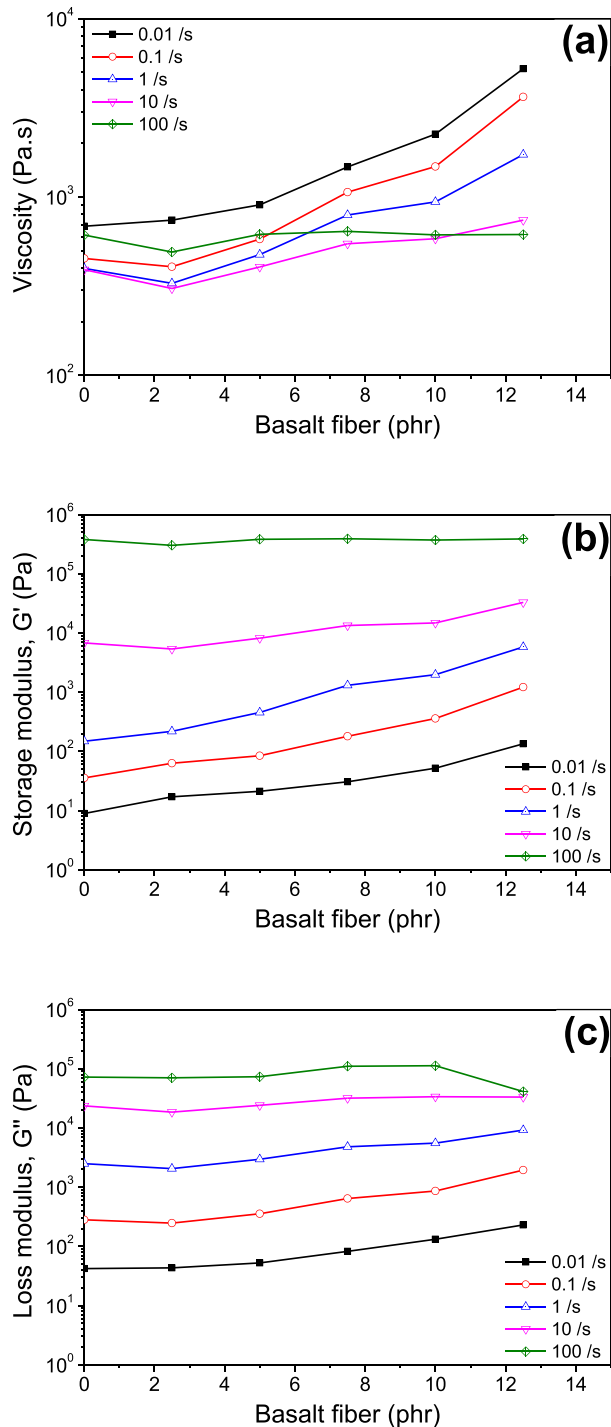


Fig. 9. Complex viscosity (a), shear storage modulus (b), and shear loss modulus (c) with different shear rates from 10^{-2} to 10^2 s^{-1} at 270 °C for neat PC matrix and composites with different PC/BF ratios up to 12.5 phr.

12.5 phr of BF concentration. The tensile and the flexural strength were also increased from 63 to 95 MPa to 83 and 126 MPa, respectively. The impact strength was decreased due to the ductile-to-brittle transition. The HDT of the PC/BF composites was increased by ca. 8 °C, which is consistent with T_g s measured by TMA whereas the T_g s by DSC were almost identical for all samples due to the difference in measurement mechanisms. The visual observation for the PC/BF composites was examined via SEM. All rheological

analysis tools used in this study showed higher viscosity at higher BF concentrations. Capillary rheometry showed shear thinning phenomenon for all composites at all shear rates and similar viscosity between the pristine PC matrix and the PC/BF composites at high shear rates. Torsional rheometry indicated the increased slope of G' vs. frequency beyond ca. 0.7 s^{-1} and a dramatic decrease in G'' at high shear rates. The BF-infiltrated polycarbonate composites can be used for various applications due to their tailorable mechanics and rheology.

Acknowledgement

This work was supported by Nano-Convergence Foundation (www.nanotech2020.org) funded by the Ministry of Science, ICT and Future Planning & the Ministry of Trade, Industry and Energy [Commercialization of 100Gbps optical receiver and transmitter modules based on nano Ag-coated Cu paste] and the Ministry of Trade, Industry & Energy (MOTIE, Korea) under Industrial Technology Innovation Program (No.10082367), [Eco-friendly Interconnection Paste and Process with Laser Bonding for Flexible LED Module].

Appendix A. Supplementary data

Supplementary data related to this article can be found at <https://doi.org/10.1016/j.polymer.2018.06.004>.

References

- X. Xu, Y. Zhang, J. Jiang, H. Wang, X. Zhao, Q. Li, W. Lu, In-situ curing of glass fiber reinforced polymer composites via resistive heating of carbon nanotube films, *Compos. Sci. Technol.* 149 (2017) 20–27, <https://doi.org/10.1016/j.compscitech.2017.06.001>.
- O. Gooranorimi, W. Suaris, E. Dauer, A. Nanni, Microstructural investigation of glass fiber reinforced polymer bars, *Compos. B Eng.* 110 (2017) 388–395, <https://doi.org/10.1016/j.compositesb.2016.11.029>.
- Y. Qin, Y. Xu, L. Zhang, G. Zheng, X. Yan, K. Dai, C. Liu, C. Shen, Z. Guo, Interfacial interaction enhancement by shear-induced β -cyclindrite in isotactic polypropylene/glass fiber composites, *Polymer* 100 (2016) 111–118, <https://doi.org/10.1016/j.polymer.2016.08.016>.
- C. Wang, M. Zhao, J. Li, J. Yu, S. Sun, S. Ge, X. Guo, F. Xie, B. Jiang, E.K. Wujcik, Y. Huang, N. Wang, Z. Guo, Silver nanoparticles/graphene oxide decorated carbon fiber synergistic reinforcement in epoxy-based composites, *Polymer* 131 (2017) 263–271, <https://doi.org/10.1016/j.polymer.2017.10.049>.
- B. Fan, Y. Liu, D. He, J. Bai, Enhanced thermal conductivity for mesophase pitch-based carbon fiber/modified boron nitride/epoxy composites, *Polymer* 122 (2017) 71–76, <https://doi.org/10.1016/j.polymer.2017.06.060>.
- G.-C. Yu, L.-Z. Wu, L.-J. Feng, W. Yang, Thermal and mechanical properties of carbon fiber polymer-matrix composites with a 3D thermal conductive pathway, *Compos. Struct.* 149 (2016) 213–219, <https://doi.org/10.1016/j.compstruct.2016.04.010>.
- L. Zhang, N. De Greef, G. Kalinka, B. Van Bilzen, J.-P. Locquet, I. Verpoest, J.W. Seo, Carbon nanotube-grafted carbon fiber polymer composites: damage characterization on the micro-scale, *Compos. B Eng.* 126 (2017) 202–210, <https://doi.org/10.1016/j.compositesb.2017.06.004>.
- P. Pötschke, T.D. Fornes, D.R. Paul, Rheological behavior of multiwalled carbon nanotube/polycarbonate composites, *Polymer* 43 (2002) 3247–3255, [https://doi.org/10.1016/S0032-3861\(02\)00151-9](https://doi.org/10.1016/S0032-3861(02)00151-9).
- J.P. Johnston, B. Koo, N. Subramanian, A. Chattopadhyay, Modeling the molecular structure of the carbon fiber/polymer interphase for multiscale analysis of composites, *Compos. B Eng.* 111 (2017) 27–36, <https://doi.org/10.1016/j.compositesb.2016.12.008>.
- V. Dhand, G. Mittal, K.Y. Rhee, S.-J. Park, D. Hui, A short review on basalt fiber reinforced polymer composites, *Compos. B Eng.* 73 (2015) 166–180, <https://doi.org/10.1016/j.compositesb.2014.12.011>.
- R. Li, Y. Gu, G. Zhang, Z. Yang, M. Li, Z. Zhang, Radiation shielding property of structural polymer composite: continuous basalt fiber reinforced epoxy matrix composite containing erbium oxide, *Compos. Sci. Technol.* 143 (2017) 67–74, <https://doi.org/10.1016/j.compscitech.2017.03.002>.
- Z. Ying, D. Wu, M. Zhang, Y. Qiu, Polylactide/basalt fiber composites with tailorable mechanical properties: effect of surface treatment of fibers and annealing, *Compos. Struct.* 176 (2017) 1020–1027, <https://doi.org/10.1016/j.compstruct.2017.06.042>.
- Y. Zhang, C. Yu, P.K. Chu, F. Lv, C. Zhang, J. Ji, R. Zhang, H. Wang, Mechanical and thermal properties of basalt fiber reinforced poly(butylene succinate) composites, *Mater. Chem. Phys.* 133 (2012) 845–849, <https://doi.org/10.1016/>

- [j.matchemphys.2012.01.105](https://doi.org/10.1016/j.matchemphys.2012.01.105).
- [14] T. Czígány, Special manufacturing and characteristics of basalt fiber reinforced hybrid polypropylene composites: mechanical properties and acoustic emission study, *Compos. Sci. Technol.* 66 (2006) 3210–3220, <https://doi.org/10.1016/j.compscitech.2005.07.007>.
- [15] K.-S. Jang, Mineral filler effect on the mechanics and flame retardancy of polycarbonate composites: talc and kaolin, *E-Polymers* 16 (2016) 379–386, <https://doi.org/10.1515/epoly-2016-0103>.
- [16] K.L. Camera, B. Wenning, A. Lal, C.K. Ober, Transient materials from thermally-sensitive polycarbonates and polycarbonate nanocomposites, *Polymer* 101 (2016) 59–66, <https://doi.org/10.1016/j.polymer.2016.08.050>.
- [17] X. Gao, A.I. Isayev, C. Yi, Ultrasonic treatment of polycarbonate/carbon nanotubes composites, *Polymer* 84 (2016) 209–222, <https://doi.org/10.1016/j.polymer.2015.12.051>.
- [18] Y. Tanaka, K. Naito, H. Kakisawa, Measurement method of multi scale thermal deformation inhomogeneity in CFRP using in situ FE-SEM observations, *Composites Part Appl. Sci. Manuf* 102 (2017) 178–183, <https://doi.org/10.1016/j.compositesa.2017.08.002>.
- [19] F. Naya, C. González, C.S. Lopes, S. Van der Veen, F. Pons, Computational micromechanics of the transverse and shear behavior of unidirectional fiber reinforced polymers including environmental effects, *Composites Part Appl. Sci. Manuf* 92 (2017) 146–157, <https://doi.org/10.1016/j.compositesa.2016.06.018>.
- [20] K. Shirvanimoghaddam, S.U. Hamim, M. Karbalaee Akbari, S.M. Fakhrhoseini, H. Khayyam, A.H. Pakseresht, E. Ghasali, M. Zabet, K.S. Munir, S. Jia, J.P. Davim, M. Naebe, Carbon fiber reinforced metal matrix composites: fabrication processes and properties, *Composites Part Appl. Sci. Manuf* 92 (2017) 70–96, <https://doi.org/10.1016/j.compositesa.2016.10.032>.
- [21] B.K. Satapathy, R. Weidisch, P. Pötschke, A. Janke, Crack toughness behaviour of multiwalled carbon nanotube (MWNT)/Polycarbonate nanocomposites, *Macromol. Rapid Commun.* 26 (2005) 1246–1252, <https://doi.org/10.1002/marc.200500234>.
- [22] X. Zhi, H.-B. Zhang, Y.-F. Liao, Q.-H. Hu, C.-X. Gui, Z.-Z. Yu, Electrically conductive polycarbonate/carbon nanotube composites toughened with micron-scale voids, *Carbon* 82 (2015) 195–204, <https://doi.org/10.1016/j.carbon.2014.10.062>.
- [23] E.T.J. Klompen, T.A.P. Engels, L.C.A. van Breemen, P.J.G. Schreurs, L.E. Govaert, H.E.H. Meijer, Quantitative prediction of long-term failure of polycarbonate, *Macromolecules* 38 (2005) 7009–7017, <https://doi.org/10.1021/ma0504973>.
- [24] T.T. Law, Y.J. Phua, R. Senawi, A. Hassan, Z.A. Mohd Ishak, Experimental analysis and theoretical modeling of the mechanical behavior of short glass fiber and short carbon fiber reinforced polycarbonate hybrid composites, *Polym. Compos.* 37 (2016) 1238–1248, <https://doi.org/10.1002/pc.23289>.
- [25] B.A. Knutsson, J.L. White, K.B. Abbas, Rheological and extrusion characteristics of glass fiber-reinforced polycarbonate, *J. Appl. Polym. Sci.* 26 (1981) 2347–2362, <https://doi.org/10.1002/app.1981.070260721>.
- [26] S.-H. Chang, J.-R. Hwang, J.-L. Doong, Optimization of the injection molding process of short glass fiber reinforced polycarbonate composites using grey relational analysis, *J. Mater. Process. Technol.* 97 (2000) 186–193, [https://doi.org/10.1016/S0924-0136\(99\)00375-1](https://doi.org/10.1016/S0924-0136(99)00375-1).
- [27] P. Chen, J. Zhang, J. He, Increased flow property of polycarbonate by adding hollow glass beads, *Polym. Eng. Sci.* 45 (2005) 1119–1131, <https://doi.org/10.1002/pen.20382>.
- [28] S.H. Hashemabadi, S.M. Mirnajafizadeh, Analysis of viscoelastic fluid flow with temperature dependent properties in plane Couette flow and thin annuli, *Appl. Math. Model.* 34 (2010) 919–930, <https://doi.org/10.1016/j.apm.2009.07.001>.
- [29] R.C. Warren, Viscous Heating, in: *Rheol. Meas.*, Springer, Dordrecht, 1998, pp. 210–236, https://doi.org/10.1007/978-94-011-4934-1_7.
- [30] S. Wolff, J.-B. Donnet, Characterization of fillers in vulcanizates according to the einstein-guth-gold equation, *Rubber Chem. Technol.* 63 (1990) 32–45, <https://doi.org/10.5254/1.3538240>.
- [31] E. Guth, Theory of filler reinforcement, *J. Appl. Phys.* 16 (1945) 20–25, <https://doi.org/10.1063/1.1707495>.
- [32] E.M. Silverman, Effect of glass fiber length on the creep and impact resistance of reinforced thermoplastics, *Polym. Compos.* 8 (1987) 8–15, <https://doi.org/10.1002/pc.750080103>.
- [33] M. DeSarkar, P. Senthilkumar, S. Franklin, G. Chatterjee, Effect of particulate fillers on thermal expansions and other critical performances of polycarbonate-based compositions, *J. Appl. Polym. Sci.* 124 (2012) 215–226, <https://doi.org/10.1002/app.33667>.
- [34] H. Liang, W. Jiang, J. Zhang, B. Jiang, Toughening mechanism of polymer blends: influence of voiding ability of dispersed-phase particles, *J. Appl. Polym. Sci.* 59 (1996) 505–509, [https://doi.org/10.1002/\(SICI\)1097-4628\(19960118\)59:3<505::AID-APP16>3.0.CO;2-S](https://doi.org/10.1002/(SICI)1097-4628(19960118)59:3<505::AID-APP16>3.0.CO;2-S).
- [35] Y. Shangguan, F. Chen, J. Yang, E. Jia, Q. Zheng, A new approach to fabricate polypropylene alloy with excellent low-temperature toughness and balanced toughness-rigidity through unmatched thermal expansion coefficients between components, *Polymer* 112 (2017) 318–324, <https://doi.org/10.1016/j.polymer.2017.02.022>.
- [36] M. Hasegawa, Y. Hoshino, N. Katsura, J. Ishii, Superheat-resistant polymers with low coefficients of thermal expansion, *Polymer* 111 (2017) 91–102, <https://doi.org/10.1016/j.polymer.2017.01.028>.
- [37] A.P.R. Eberle, D.G. Baird, P. Wapperom, Rheology of Non-Newtonian fluids containing glass fibers: a review of experimental literature, *Ind. Eng. Chem. Res.* 47 (2008) 3470–3488, <https://doi.org/10.1021/ie070800j>.
- [38] F. Kern, R. Gadow, Extrusion and injection molding of ceramic micro and nanocomposites, *Int. J. Material Form.* 2 (2009) 609–612, <https://doi.org/10.1007/s12289-009-0487-8>.
- [39] I.H. Baick, Y. Ye, C.V. Luciani, Y.G. Ahn, K.H. Song, K.Y. Choi, UltraHigh molecular weight nonlinear polycarbonates synthesized in microlayers, *Ind. Eng. Chem. Res.* 52 (2013) 17419–17431, <https://doi.org/10.1021/ie4029544>.
- [40] R.K. Bregg, *Frontal Polymer Research*, Nova Publishers, 2006.
- [41] K.S. Cole, R.H. Cole, Dispersion and absorption in dielectrics I. Alternating current characteristics, *J. Chem. Phys.* 9 (1941) 341–351, <https://doi.org/10.1063/1.1750906>.
- [42] H.-K. Chuang, C.D. Han, Rheological behavior of polymer blends, *J. Appl. Polym. Sci.* 29 (1984) 2205–2229, <https://doi.org/10.1002/app.1984.070290625>.
- [43] C.D. Han, J. Kim, J.K. Kim, Determination of the order-disorder transition temperature of block copolymers, *Macromolecules* 22 (1989) 383–394, <https://doi.org/10.1021/ma00191a071>.
- [44] E.R. Harrell, N. Nakajima, Modified Cole–Cole plot based on viscoelastic properties for characterizing molecular architecture of elastomers, *J. Appl. Polym. Sci.* 29 (1984) 995–1010, <https://doi.org/10.1002/app.1984.070290327>.
- [45] C. Dae Han, Measurement of the rheological properties of polymer melts with slit rheometer. III. Two-phase systems—high-impact polystyrene and ABS resin, *J. Appl. Polym. Sci.* 15 (1971) 2591–2596, <https://doi.org/10.1002/app.1971.070151024>.